A Solar Thermophotovoltaic Electrical Generator for Remote Power Applications

NAS3–27779
Final Report

Contractor –
Essential Research, Inc.
2460 Fairmount Blvd.
Suite A
Cleveland, OH 44106

Authored by –
Navid S. Fatemi

February 12, 1996

ESSENTIAL RESEARCH INCORPORATED

This effort is funded by the Ballistic Missile Defense Organization Small Business Innovation Research Program, and administered by the NASA Lewis Research Center.

A Solar Thermophotovoltaic Electric Generator for Remote Power Applications

Table of Contents

1. Project Summary 1

2. Background 2

3. Experimental Procedures 4

3.1. Selective Emitter Characterization 4

3.2. Filter Characterization 5

3.3. PV Cell Growth and Fabrication 5

3.4. PV Cell Hydrogen Passivation 8

3.5. Converter Testing 8

4. Results 11

4.1. Ho-YAG, Tm-(Lu,YAG), and Er-YAG Selective Emitter Emittance Data 11

4.2. Bandpass/IR Reflector Filter Optical Characterization Data 12

4.3. PV Cell Performance 14

4.3.1. AM0 I-V Data 15

4.3.2. Spectral Response and Quantum Efficiency Data 15

4.3.3. High light Injection I-V Data 17

4.3.4. Hydrogen Passivation Data 19

4.4. Thermal Storage 20

4.5. Stirling Solar Concentrator Dish Test Results 22

4.5. Emitter, Bandpass/IR Reflector Filter, and PV Cell Converter Test Results 22

4.6.1 Ho-YAG Selective Emitter, Filter, and PV Cell with Eg=0.51 eV 24

4.6.2 Tm-Lu,YAG Selective Emitter, Filter, and PV Cell with Eg=0.57 eV 26

4.6.3 Er-YAG Selective Emitter, Filter, and PV Cell with Eg=0.69 eV 27

4.6.4 Blackbody Broadband Emitter, Filter, and PV Cell with Eg=0.69 eV 29

5. Conclusions 32

6. Future Research and Development 33

7. References 35

A Solar Thermophotovoltaic Electric Generator for Remote Power Applications

1. Project Summary

The goal of the this SBIR project is to develop a technology to enable high-efficiency solar thermophotovoltaic (STPV) energy conversion. All Phase I technical objectives were successfully met or surpassed. We demonstrated TPV energy conversion by developing converters consisting of rare-earth-doped yttrium aluminum garnet (YAG) and lutetium yttrium aluminum garnet (Lu,YAG) selective emitters and a blackbody emitter, bandpass/infrared (IR) reflector filters, and InGaAs photovoltaic (PV) cells. The PV cells were grown via organometallic vapor phase epitaxy (OMVPE). The operating temperature of the heat source was 1700 K.

STPV converter efficiencies approaching 30%, as well as electrical output power densities near 2 W/cm^2 were demonstrated. Specifically, we accomplished the following:

1. measured the spectral emittance of Ho-doped and Er-doped YAG, as well Tm-doped Lu,YAG selective emitters
2. designed, acquired, and tested bandpass filters (on sapphire) with cutoff wavelengths at 2.0 and 2.2 μm
3. fabricated PV cells with energy bandgaps (Eg) in the range of 0.51 to 0.69 eV by growing InGaAs on InP substrates by OMVPE
4. investigated the effect of hydrogen passivation on the performance of lattice-mismatched InGaAs on InP
5. extensively investigated and found a suitable technology for an STPV thermal storage receiver/emitter unit
6. demonstrated receiver operating temperatures in excess of 1500 K for a Stirling solar concentrator dish located at the solar testing facilities of McDonnell Douglas Aerospace
7. demonstrated a TPV converter efficiency of 11.4% for a converter consisting of a Ho-doped YAG selective emitter, a bandpass/IR reflector filter, and a PV cell with Eg=0.51 eV. The electrical output power density for this converter was 0.29 W/cm^2

8. demonstrated a TPV converter efficiency of 16.2% for a converter consisting of a Tm-doped Lu,YAG selective emitter, a bandpass/IR reflector filter, and a PV cell with Eg=0.57 eV. The electrical output power density for this converter was 0.44 W/cm^2

9. demonstrated a TPV converter efficiency of 29.0% for a converter consisting of an Er-doped YAG selective emitter, a bandpass/IR reflector filter, and a PV cell with Eg=0.69 eV. The electrical output power density for this converter was 0.78 W/cm^2

10. demonstrated a TPV converter efficiency of 26.9% for a converter consisting of a blackbody emitter, a bandpass/IR reflector filter, and a PV cell with Eg=0.69 eV. The electrical output power density for this converter was 1.94 W/cm^2.

The following conclusions may be drawn from our research:

1. Practical high-efficiency, high output power density converters can be realized for STPV applications.

2. Although the center of the emission peak for the Tm-doped Lu,YAG selective emitter was most optimally matched to the blackbody spectral irradiance curve to produce the highest output power at 1700 K, the converter with the Er-doped YAG selective emitter produced a significantly higher output power density (and efficiency). This was mainly due to the fact that the performance of the PV cell in the latter converter (Eg=0.69 eV) was significantly better than the performance of the cell in the former converter (Eg=0.57 eV).

3. Since existing selective emitters have radiative efficiencies in the 20–30% range, additional filtering elements are needed to achieve high converter efficiencies. The combination of a selective emitter and a filter, however, results in relatively low output power densities (i.e., <1 W/cm^2).

4. The filtered blackbody-based converter, on the other hand, exhibits a high output power density (~2 W/cm^2), while maintaining a high efficiency (26.9%). Furthermore, the radiation recycling efficiency of this converter, due to filtering, is expected to be far better than selective emitter-based converters.

Based on the above conclusions, the proposed STPV prototypes planned for the Phase II contract will be built with filtered blackbody-based TPV converters.

2. Background

Remote power generation is an important technology for space-based missions, military ground operations, and operations other than war, such as delivering humanitarian and peacekeeping aid to underdeveloped countries. Currently, thermopiles, fueled by radioisotope heat sources, are used for deep-space exploration. NASA desires to abandon this technology, however, because of the perceived environmental threat. In military and humanitarian operations, thermionic or diesel generators are used to provide power. Thermionic generators are inefficient and costly to operate. Particularly when the cost of transporting fuel is high, the use of thermionic generators results in very expensive power. Currently the Air Force spends upwards of $175,000 annually to deliver 60 W of power to remote sensing outposts in Alaska, for example. Diesel generators are efficient, but are heavy, noisy, polluting, and consuming of nonrenewable energy. In addition, they require constant maintenance and are typically not practical when a degree of mobility is required, as is sometimes the case in humanitarian and peacekeeping missions.

Thermophotovoltaic energy conversion (TPV) is a technology well-suited for the development of highly-efficient, compact, and reliable sources of electricity. In TPV energy conversion, heat is first converted to radiant energy by a selective emitter, then to electrical energy by a photovoltaic (PV) cell. For optimal efficiency, the PV cell must have a narrower bandgap than the traditional Si and GaAs cells used for converting the solar spectrum. Currently, TPV systems are under development, by us and others, utilizing radioisotope and gaseous or liquid combustion heat sources. These approaches have their drawbacks, including (1) the environmental hazard of nuclear materials, (2) the production of NO_X emissions, (3) the consumption of nonrenewable energy, (4) a limited duration of power production, (5) the production of soot, which potentially degrades system performance, and (6) the need for extensive advances in combustor technology to achieve safe, reliable, and compact heat sources.

Solar thermophotovoltaic (TPV) power generation uses concentrated sunlight as the heat source for TPV conversion. The sun is concentrated and used to heat a thermal absorber. Thermal radiation, and not the solar spectrum, is then converted to electricity with a narrow bandgap PV cell. This concept has been pioneered at McDonnell Douglas Aerospace, who have shown that solar-heated TPV has great potential for supplying large amounts of electricity to the utilities.[1] In addition to efficient energy conversion, solar TPV offers the element of energy storage; power can be produced after sun down, during cloud cover, or continuously during space orbit. Although originally conceived of for commercial application and capable of supplying kilowatts of electricity, solar TPV can easily be scaled down to produce tens or hundreds of watts as needed in mobile or remote power generation. Likewise, it has a high power-to-mass ratio and can thus be configured for use in space exploration.

The use of concentrated solar energy as a heat source does not have the drawbacks associated with radioisotope or combustion heat sources. A very pragmatic advantage of solar power is that dish concentrators are a well-developed technology. Therefore, the development effort and time to market, relative to other TPV concepts, will be reduced. It is the only TPV approach based upon a renewable energy source. In addition, solar TPV has no moving parts, is light weight, and produces no noise or vibration. It has the potential to be extremely reliable.

Solar TPV is projected to be cost competitive with traditional means of photovoltaic power generation for supplying large amounts of power to utilities. The McDonnell Douglas study projects that solar TPV will be both more efficient, and less costly to operate, than the Kinematics Stirling Dish. It has the potential to greatly reduce the cost of remote power generation for some military operations. When scaled down for remote applications, solar TPV is expected to be at least twice as efficient as thermionic generators. For deep space exploration, solar TPV may be the only practical replacement to radioisotope heat sources. Even with a large thermal storage system capable of maintaining constant power output during the orbit night, the mass would be less than a space solar dynamic system. With no moving parts, solar TPV offers high reliability required for space operation and the low operating and maintenance cost required for utility operation. Importantly, the solar TPV system can be shielded to eliminate degradation due to radiation.

3. Experimental Procedures

3.1. Selective Emitter Characterization

The Ho-YAG, Tm-(Lu,YAG), and Er-YAG selective emitters were characterized using a custom developed test bed designed for measuring thin-film selective emitters for thermo-photovoltaic applications. A schematic representing the experimental configuration is shown in figure 1.

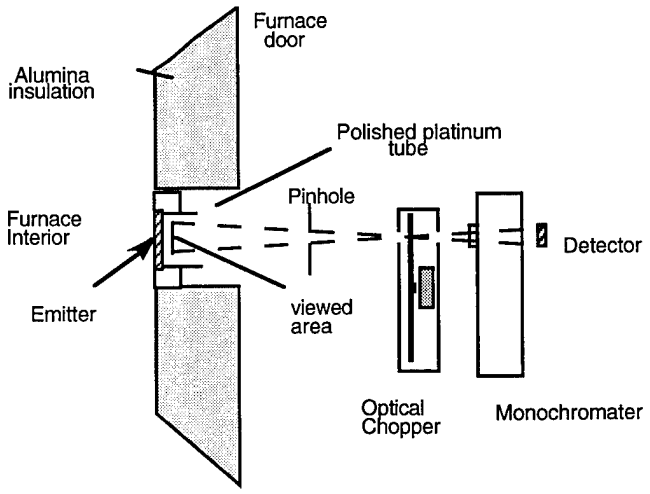

Figure 1.—Schematic diagram of experimental setup for measuring emission spectra.

Since significant temperature differences (160–180 K) exist between the front and back emitter surfaces, the "emitter temperature" is defined by a substrate temperature (T_S), and the temperature gradient, $\Delta T = T_S - T_{Front}$. The average of the front and back surface temperatures, $T_{avg} = (T_S - T_{Front})/2$, in the center of the sample is used to calculate the spectral emittance from the spectroradiometer intensity measurements. Temperatures were measured with type R thermocouples to an accuracy of ±6 K. Normal spectral emittance measurements were made from 1.2–3.2 μm with a spectroradiometer constructed from a 1/8-meter monochrometer, a

temperature-controlled PbS detector, and an 800-Hz chopper. The spectroradiometer was calibrated with a 1273 K blackbody reference.

3.2. Filter Characterization

Filter characterization was carried out by testing the filters with a Perkin-Elmer Lambda 19 spectrophotometer and a Nicolet Magna-IR 750 FTIR spectrometer. Although the Lambda 19 spectrophotometer is able to make more accurate measurements than the FTIR spectrometer, its wavelength range of data gathering is more limited, i.e. 0–3 versus 0–30 μm. Consequently, measurements were made using both instruments.

Transmission, reflectance, and absorptance versus wavelength was measured for two types of filters. One was an IR reflector filter. It is fabricated by the deposition of a thin layer of gold (~50Å) on a sapphire substrate. The second was a dielectric stack on sapphire bandpass filter. Three bandpass filters were tested with cutoff wavelengths of 2.2, 2.0, and 1.7 μm. Measurements were also taken for the combination: bandpass/IR reflector filters. These combination filter configurations were ultimately used in TPV converter testing.

3.3. PV Cell Growth and Fabrication

A fast switching, horizontal, low-pressure OMVPE reactor was employed for all semiconductor material growth. The reactant species were trimethylindium (TMIn), trimethylgallium (TMGa), diethylzinc (DEZn), phosphine (PH_3), arsine (AsH_3) and silane (SiH_4). Hydrogen carrier gas was used to inject the precursors into the reaction chamber. Substrates were placed on a SiC-coated graphite susceptor. Growth conditions for the various layers are presented in Table I. Samples were characterized for crystal quality, alloy composition, and surface morphology using double x-ray diffraction (DCXRD), visual observations, and Normarski contrast optical microscopy.

$In_xGa_{1-x}As$ layers were grown on p-type InP wafers, which were prepared by the substrate vendor. A thin layer of InP was first grown on all substrates to provide a clean surface for nucleation of the InGaAs alloys. A lattice-matched InGaAs layer with Eg=0.74 eV was then grown directly on the InP layer. Lattice-mismatched InGaAs structures with Eg=0.51, 0.57 and 0.69 eV were grown on the lattice-matched InGaAs layer. Compositionally stepped buffer layer were grown to reduce the number of threading dislocations in the active cell base region. Step compositions were chosen to keep the strain below 0.2125% between every two layers. Thus, five equal compositional steps were in the buffer for the cell with Eg=0.57 eV, and eight steps composed the buffer for the cell with Eg=0.51 eV. The cell with Eg=0.69 eV was grown without any intermediate buffers. Finally, all cell structures were capped with InP. The InP cap was 0.5 μm thick for the cell with Eg=0.69 eV, and 0.05 μm thick for the cells with Eg=0.57 and 0.51 eV. Growth temperature and pressure were 620 °C and 190 torr throughout all OMVPE runs. Growth conditions for the various alloys are summarized in Table I.

Table I.–OMVPE growth conditions for the InGaAs/InP PV cells.

Alloy	TMIn µmol/min.	TMGa µmol/min.	PH_3 µmole/min.	AsH_3 µmole/min.	Growth Rate nm/sec
0.51 eV InGaAs	39.8	8.6	–	1636	1.43
0.57 eV InGaAs	25.5	8.6	–	1636	1.06
0.69 eV InGaAs	14.8	8.6	–	1636	0.78
InP	25.5	–	1145	–	0.65

The OMVPE grown cell structures were processed into PV cells using the following procedure:

1. Back Contacts: Low-resistance ohmic contacts made by vacuum depositing a sandwich of Au-Zn-Au on the p^+-InP substrates, and heat treating in the range of 400–440 °C.[2] The contacts were typically 2–3 µm thick.

2. Front Contacts: Standard reverse-imaging photolithography was used to define the grid geometry of the front contacts. Thermally stable, low-resistance ohmic contacts made by vacuum depositing a sandwich of Au-Ge-Au on the n^+-InP window layers.[3] Front contacts were typically 2.5–3 µm thick. The optimized front grid geometries for these cells is shown in figure 2. The grid shadowing (GS) for both geometries was 20%.

3. Mesa Isolation: Standard photolithography was used to define the cell area. The defined areas were isolated via chemical etching using HCl-based and H_2SO_4-based solutions. The cross-sectional views of the finished cells are shown in figure 3.

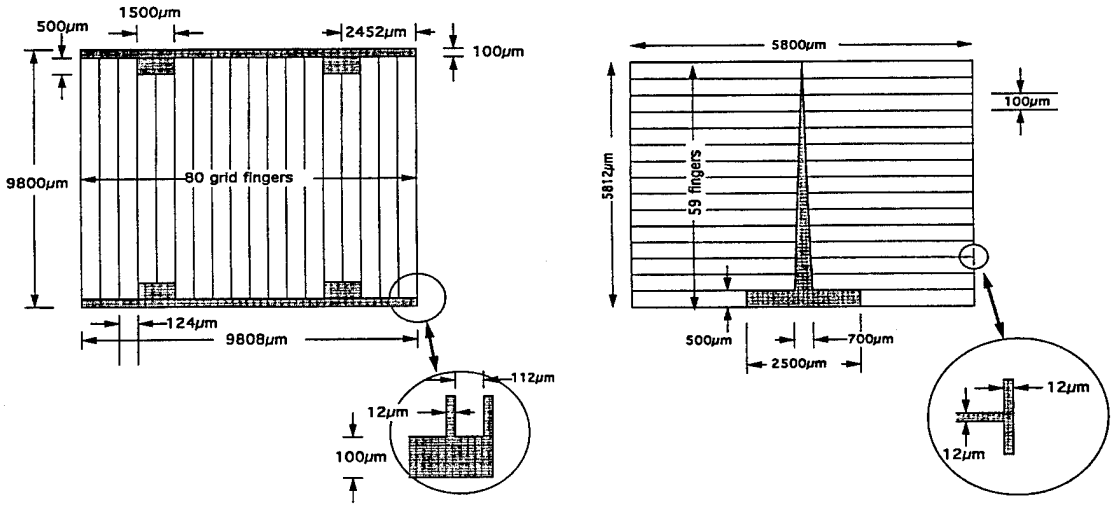

Figure 2.—Front grid design for the 1x1 cm (left), and the 6x6 mm (right) PV cells.

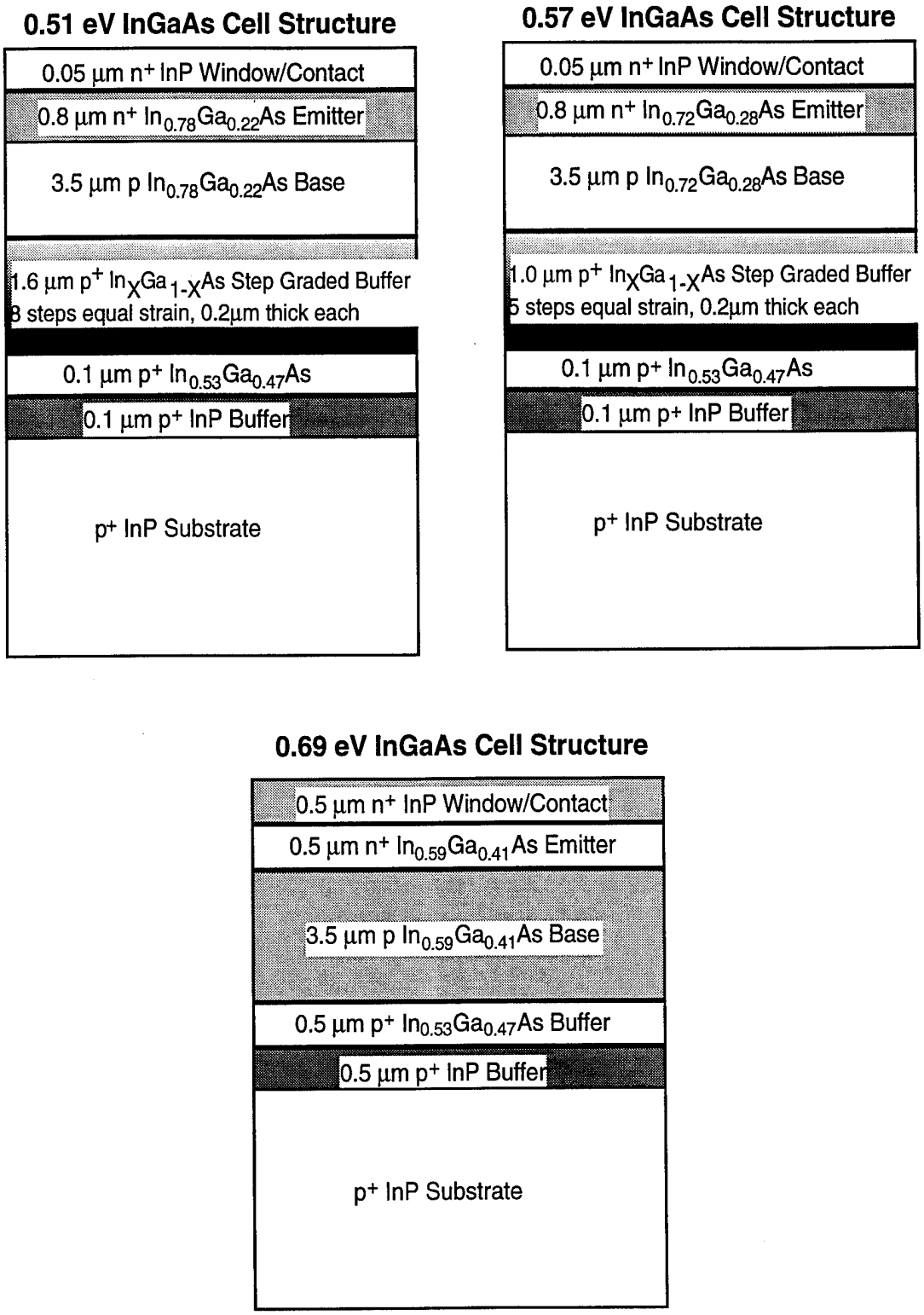

Figure 3.—Cross-sectional view of fabricated InGaAs photovoltaic cells.

In addition, several transmission line model (TLM) test pads were fabricated in close proximity to the PV cells. TLM test pads furnished important electrical data about the ohmic contact metallization and the n^+/n^+ InP/InGaAs cell emitter, such as metal-semiconductor specific contact resistivity (r_C) and the semiconductor emitter sheet resistivity (R_{SH}). The as-fabricated r_C values for the Au-Ge contacts were in the low 10^{-6} to low 10^{-8} Ω-cm^2 range. The emitter sheet resistivities for all cells varied from 8 to 11 Ω/sq.

3.4. PV Cell Hydrogen Passivation

The processes of PV cell hydrogenation was carried out in the following steps:

1. Acetone and methanol organic cleaning with ultrasonic agitation.
2. HF:H_2O (1:10 vol.) surface cleaning for 15 seconds.
3. Deposition of a SiNx (200 Å) protective layer at 275 °C.
4. Hydrogenation at 250 °C for 2 hr in a Technics Planar Etch II parallel plate, 13.56 MHz plasma reactor. The hydrogen flow rate was 30 sccm at a power density of 0.08 W/cm^2, and chamber pressure of 750 m Torr.
5. Dopant reactivation annealing at 400 °C for 5 min in a nitrogen ambient.
6. Removal of the SiNx layer in HF:H2O (1:10 vol.) in 5 min.

3.5. Converter Testing

Figure 4 is a schematic illustration of a TPV converter. All converters were tested by first carefully characterizing and testing each of their components separately. All of the measured parameters were then combined, in the methodology described below, to obtain converter output power density and efficiency values.

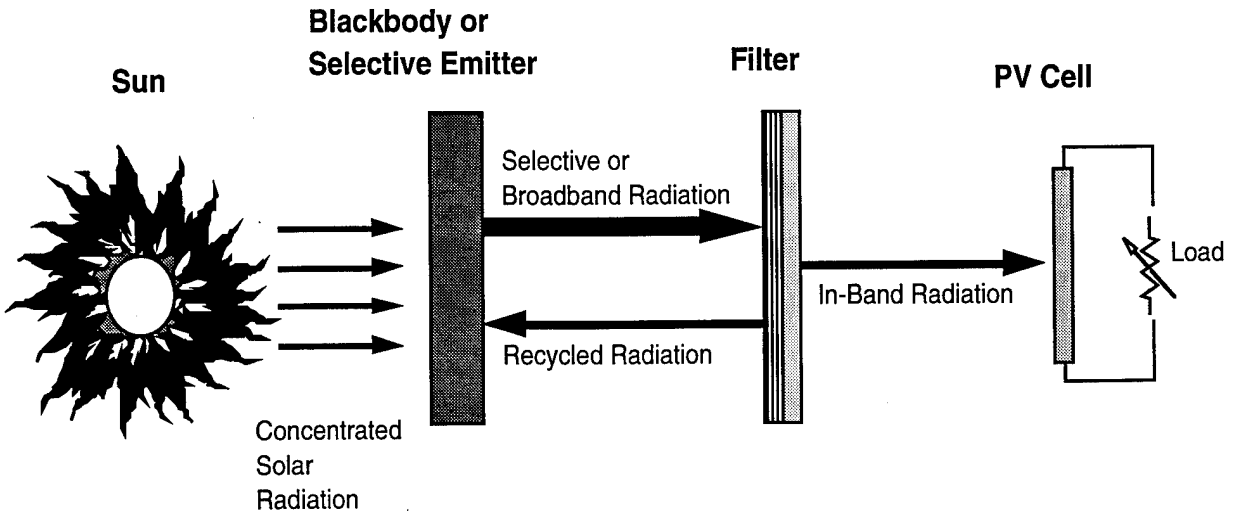

Figure 4.—Schematic representation of the TPV process.

First, the spectral irradiance (W/cm^2) of each selective emitter, as a function of wavelength, was calculated by multiplying the measured spectral emittance of the selective emitter by the well-known blackbody spectral irradiance (at 1700 K). The measured transmission versus wavelength of every bandpass/IR reflector filter was then multiplied by the respective selective emitter spectral irradiance. The result was the filtered spectral irradiance reaching the PV cell. The current output density (A/cm^2) of the PV cell was then calculated by integrating the product of the measured cell spectral response (A/W) and the filtered spectral irradiance over the wavelength range of interest, i.e. from near zero microns to the cutoff wavelength (λ_c) of the bandpass filter.

The open-circuit voltage (V_{oc}) and fill factor (FF) values of the PV cells were measured at the output short-circuit current (J_{sc}) levels calculated above, by testing the cells under high sunlight concentrations, using a large-area pulsed solar simulator (LAPSS). This ensured accurate V_{oc} and FF measurements because the detrimental effects of cell series resistance were experimentally taken into account. The cell output power density (W/cm^2) was then simply calculated as the product of V_{oc}, J_{sc}, and FF.

In order to calculate the converter efficiency, the cell power output density calculated above was divided by the total selective emitter spectral irradiance, integrated over the wavelength range of interest. A 100% radiation recycling was assumed with all converters. The Excel 5.0 program was used to model, as well as to perform matrix calculations to obtain the desired results. The parameters, symbols, and definitions used for this program are presented in worksheet I.

Worksheet I.—Parameters used for TPV converter calculations.

System-level Inputs

Variable	Description	Units	Notes
Psys	power output, total system	W	
Top	operating temperature	K	
GFF	geometric focusing factor	dimensionless	=Aarray/Aemitter

System-level Calculated Outputs

Variable	Description	Units	Equation
η_{TPV}	efficiency, TPV converter	dimensionless	$=P_{emitter}/P_{sys}$

Absorber Inputs

Variable	Description	Units	Notes
Absorber	type	text	
$Spec_{absorb}$	specification	text	
ε_{absorb}	emissivity	dimensionless	blackbody

Absorber Calculated Outputs

Variable	Description	Units	Equation
$e_{absorb}(\lambda)$	emissive power	W/(μm cm^2)	$=\varepsilon_{absorb} * C_1/\lambda^5 * (1/\exp(C_2/\lambda T_{op}-1))$
q_{absorb}	total emissive power	W/cm^2	$=\int e_{absorb}(\lambda)\, \partial\lambda$
P_{absorb}	total emitted power	W	$=q_{absorb} * A_{absorb}$
$e_{emitter}(\lambda)$	emissive power	W/(μm cm^2)	$=e_{absorb}(\lambda)$
$q_{emitter}$	total emissive power	W/cm^2	$=q_{absorb}$
$P_{emitter}$	total emitted power	W	$=P_{absorb}$
A_{absorb}	area	cm^2	$=A_{emitter}$
$A_{emitter}$	area	cm^2	$=A_{array}/GFF$

Filter Inputs

Variable	Description	Units	Notes
Filter	type	text	
$Spec_{filter}$	specficiation	text	
A_{filter}	area	cm^2	
$T_{filter}(\lambda)$	transmission	dimensionless	
$R_{filter}(\lambda)$	reflection	dimensionless	

Filter Calculated Ouputs

Variable	Description	Units	Equation
$a_{filter}(\lambda)$	absorption	dimensionless	$=1- T_{filter}(\lambda)- R_{filter}(\lambda)$
$e_{into\_cell}(\lambda)$	emissive power	W/(μm cm^2)	$=e_{emitter}(\lambda) * T_{filter}(\lambda)$

PV Cell Inputs

Variable	Description	Units	Notes
Cell	type	text	
$Spec_{cell}$	specification	text	
E_g	bandgap	eV	
A_{cell}	area	cm^2	
W_{cell}	weight	g	
T_{cell}	temperature	K	
$SR_{cell}(\lambda)$	spectral response	A/(μm W)	
V_{oc}	open-circuit voltage	V	
FF	fill factor	dimensionless	
GSF	grid shadowing factor	dimensionless	
PF	packing factor (cell-array)	dimensionless	

PV Cell Calculated Outputs

Variable	Description	Units	Equation
J_{sc}	short-circuit current	A/cm^2	$=\int (SR_{cell}(\lambda) * e_{into\_cell}(\lambda))\, \partial\lambda$ [from 0-2 μm]
J_{sc_arc}	short-circuit current w/AR coat	A/cm^2	$=J_{sc} * 1.35$
q_{cell}	power-output density	W/cm^2	$= J_{sc\_arc} * V_{oc} * FF$
N_{cell}	number of cells	dimensionless	$=int (P_{sys}/(q_{cell} * A_{cell} * GSF) + 1)$
A_{array}	area, array	cm^2	$=N_{cell} * A_{cell} * PF$

4. Results

4.1. Ho-YAG, Tm-(Lu,YAG), and Er-YAG Selective Emitter Emittance Data

Three different rare-earth-doped, single-crystal YAG-based selective emitters were used in this study. The first one was doped to 25% with Ho (Ho-YAG), the second was doped to 30% with Tm (Tm-Lu,YAG), and the third was doped to 40% with Er (Er-YAG). The thickness of these selective emitters were 1.1, 1.1, and 0.9 mm, respectively. All were backed with a platinum foil substrate and tested at an average emitter temperature of 1700 K. Figures 5–7 show the measured spectral emittance versus wavelength for the above selective emitters.

As shown in the figures, the peak value of the emittance in the emission band for all of the emitters was about 0.7. The overall radiative efficiencies for these emitters were in the 20-25% range.

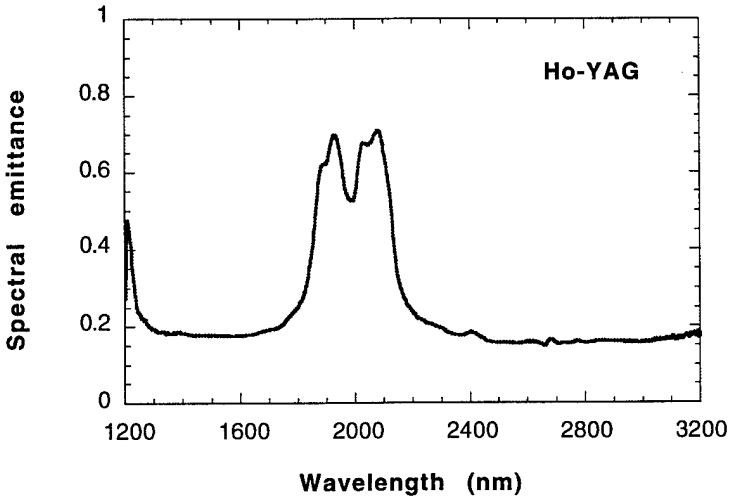

Figure 5.—Spectral emittance of a 25% Ho-doped YAG selective emitter.

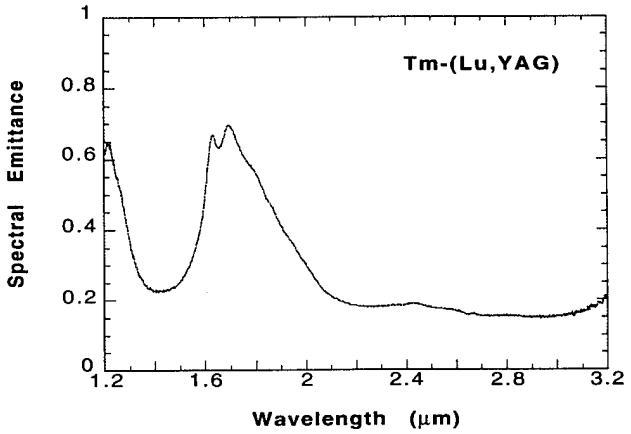

Figure 6.—Spectral emittance of a 30% Tm-doped Lu,YAG selective emitter.

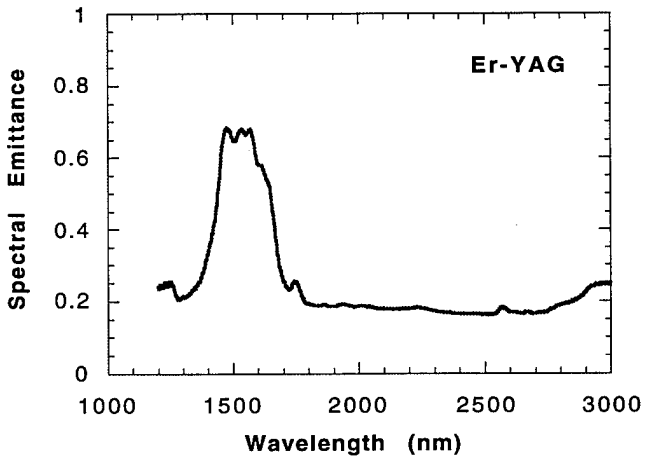

Figure 7.—Spectral emittance of a 40% Er-doped YAG selective emitter.

4.2. Bandpass/IR Reflector Filter Optical Characterization Data

Two types of filters were used to enhance the efficiency of the converters by recycling the out-of-band radiation emitted from the emitters. The first was an IR reflector filter. It served to reflect longer IR radiation back to the heat source. The transmission versus wavelength characteristics of this filter is shown in figure 8. As shown, the filter allows the transmission of most of the shorter wavelength IR radiation (in the useful range for TPV), and reflects most of the longer wavelength IR radiation. However, the transmission characteristics of this filter is a relatively smooth function of wavelength.

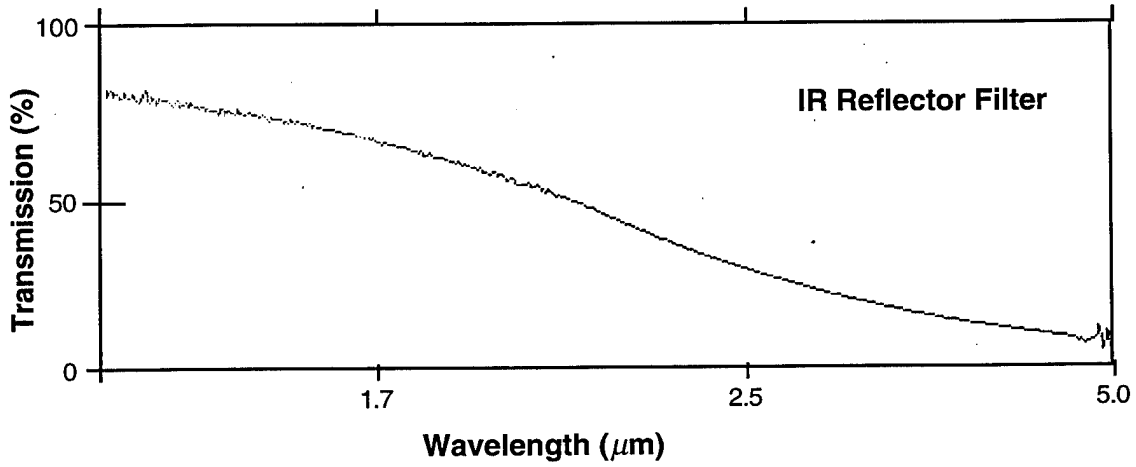

Figure 8.—Transmission characteristics of a gold-on-sapphire IR reflector filter.

Bandpass filters, on the other hand, show a near step-function behavior in their transmission versus wavelength characteristics. They transmit most of the in-band radiation up to a cutoff wavelength (λ_c), and abruptly reflect radiation beyond the cutoff wavelength. The transmission versus wavelength characteristics of a bandpass filter with (λ_c=1.7 μm) is shown in

figure 9. However, unlike the IR reflector filters, bandpass filters show significant transmission again at wavelengths >2.5 μm (see figure 9). When the bandpass filter is used in a converter configuration, this additional transmission at longer wavelengths greatly limits the converter efficiency.

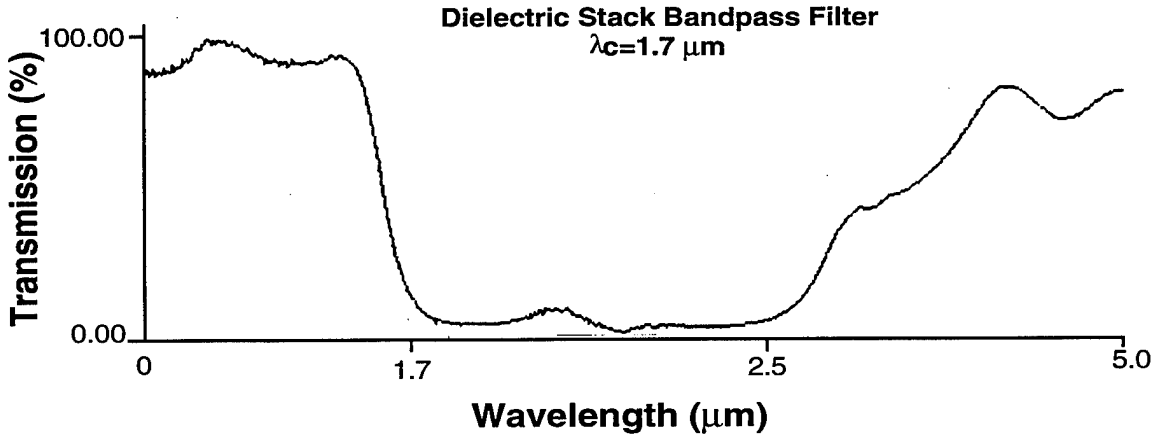

Figure 9.—Transmission characteristics of a bandpass filter with λ_c=2.0 μm.

Combining the bandpass and IR reflector filters produces the most efficient filtering for TPV applications by preserving λ_c at a desired value, while at the same time suppressing longer IR wavelength transmission. Three bandpass/IR reflector combination filters were used with cutoff wavelengths matching the peak emission bands of the selective emitters. Filters with λ_c=2.2, 2.0, and 1.7 μm, are matched to the emission peaks of the Ho-YAG, Tm-(Lu,YAG), and Er-YAG, respectively. The transmission versus wavelength characteristics for these filters are shown in figures 10-12.

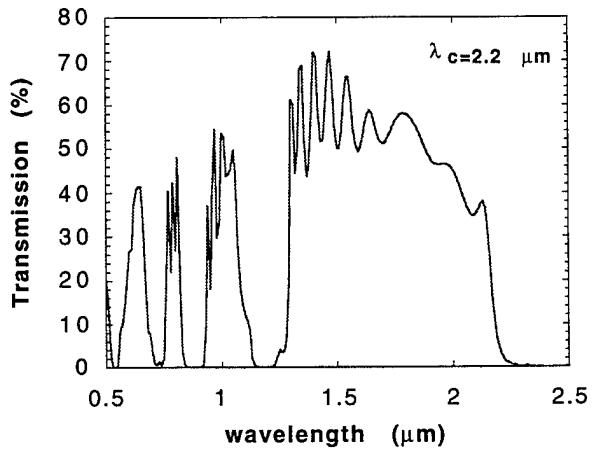

Figure 10.—Transmission characteristics of a bandpass/IR reflector filter with λ_c=2.2 μm.

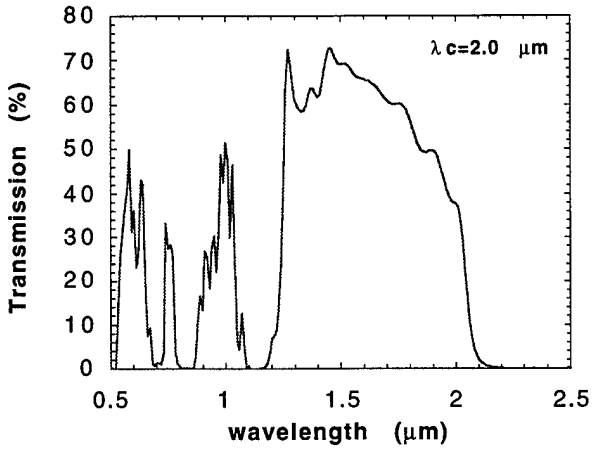

Figure 11.—Transmission characteristics of a bandpass/IR reflector filter with λ_c=2.0 μm.

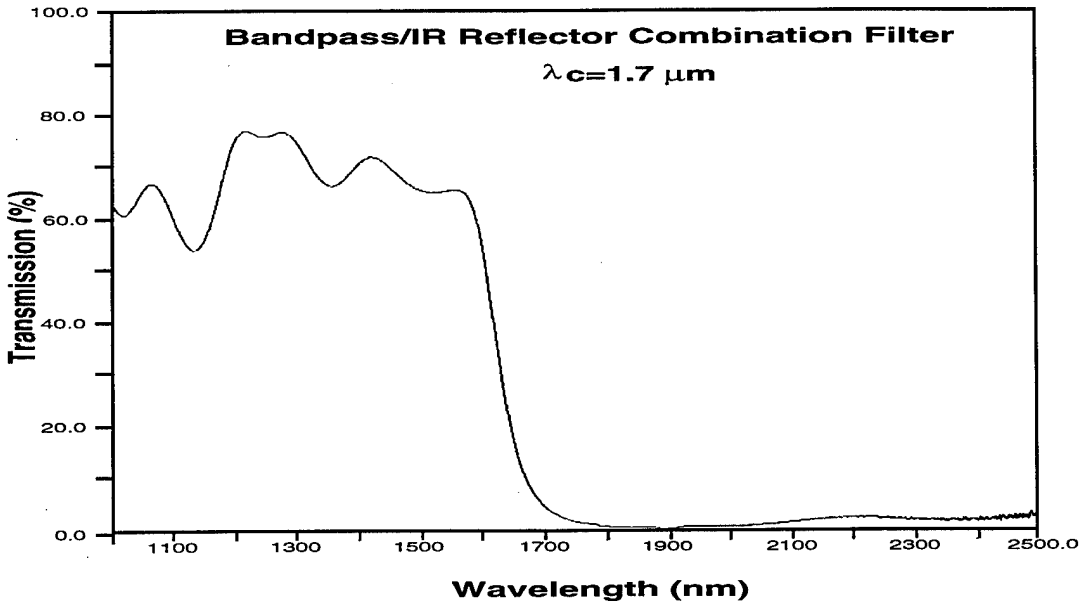

Figure 12.—Transmission characteristics of a bandpass/IR reflector filter with λ_c=1.7 μm.

4.3. PV Cell Performance

Over 30 InGaAs/InP PV cells were fabricated with bandgaps of 0.51, 0.57, and 0.69 eV. These bandgap values are well-tuned to the emission peak values of the Ho-YAG, Tm-(Lu,YAG), and Er-YAG selective emitters, respectively. The current-voltage (I-V) characteristics of each cell was initially tested under air-mass zero (AM0) conditions. Cell spectral response and quantum efficiency measurements were then performed so that the results would be used in converter efficiency calculations (see section 3.5). These measurements also

served as diagnostic measures to evaluate cell quality. Finally, the cells were tested under high light injection using a LAPSS system. The details of the results of these measurements are presented below.

4.3.1. AM0 I-V Data

Illuminated I-V testing under AM0, one-sun conditions was performed to assess the general quality of the fabricated PV cells. Particularly, the values obtained for V_{oc} and FF can, to a large extent, reveal the quality of the n/p junction. V_{oc} and FF values for cells with a given bandgap, for example, can be readily compared to those for the state-of-the-art cells. In addition, shorted or shunted cells, or cells with excessively high series resistance (Rs) can be quickly identified under AM0 testing. Table II is a summary of the AM0 I-V data for the best cells with bandgaps of 0.51, 0.57, and 0.69 eV. The cell with Eg=0.69 eV had a 2400 Å thick Ta_2O_5 anti-reflection (AR) coating, whereas the cells with Eg=0.51 and 0.57 eV had no AR coating.

Table II.—AM0, one-sun (25 °C) I-V data for best PV cells with various bandgaps.

PV Cell Eg (eV)	J_{sc} (mA/ cm^2)	V_{oc} (mV)	FF (%)	Area (cm^2)
0.51	21.0	134	48.8	0.36
0.57	31.2	226	64.4	0.36
0.69	27.6	349	69.7	1.00

As expected, the performance of the cells improve significantly as their bandgap increase. The data in Table II also show that the for the given illumination level (i.e. AM0) and bandgap, the V_{oc} and FF values are exceptionally good for all three cells. These cells were subsequently used for converter testing.

4.3.2. Spectral Response and Quantum Efficiency Data

The results of the spectral response data taken for the PV cells shown in Table II were used to calculate the output power density and efficiency for all converters. Both the spectral response and quantum efficiency curves for these cells are shown in figures 13–15. As expected, the peak value of the flat region of the quantum efficiency curves increased with increasing Eg. Also, The quantum efficiency data for all three cells are remarkably flat over a wide range of wavelengths. This is again an indication of the high quality of the cells, and the effectiveness of the buffer layers grown between the InP and the InGaAs cell structures (see section 3.3).

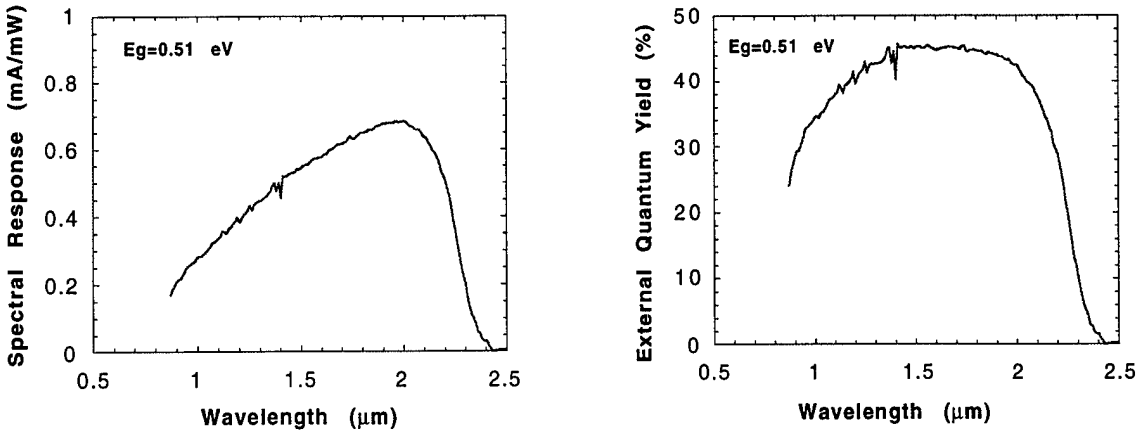

Figure 13.—Spectral response and external quantum yield for the cell with Eg=0.51 eV (no AR coating).

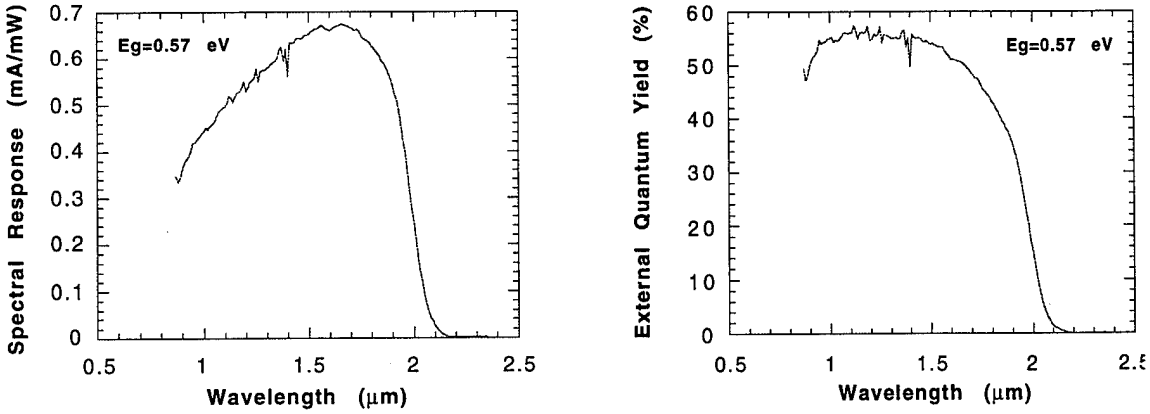

Figure 14.—Spectral response and external quantum yield for the cell with Eg=0.57 eV (no AR coating).

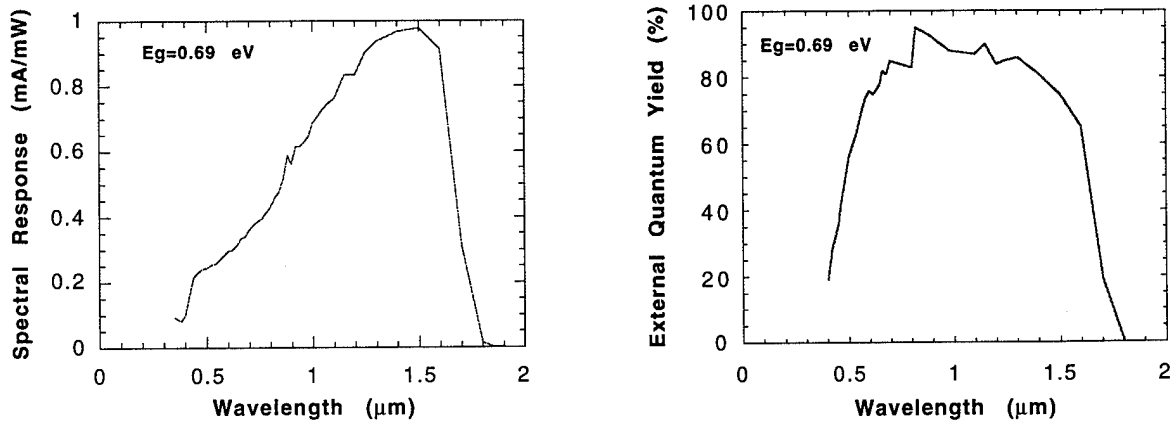

Figure 15.—Spectral response and external quantum yield for the cell with Eg=0.69 eV (Ta_2O_5 AR coating).

4.3.3. High light Injection I-V Data

In order to experimentally measure the effects of the series resistance on FF (and to a lesser extent on V_{oc}), the PV cells were subjected to high light concentration levels, using a LAPSS system. The light concentration levels were chosen such that the J_{sc} of each cell would be equal to that calculated for each of the four converters tested (see section 3.5). The results are shown in Table III. The V_{oc} and FF values shown in the table were used in converter output power density and efficiency calculations.

Table III.—High injection I-V data (25 °C) for PV cells with Eg=0.51-0.69 eV.

PV Cell Eg (eV)	J_{sc} (A/cm^2)	V_{oc} (mV)	FF (%)	Area (cm^2)
0.51	2.05	252	56.0	0.36
0.57	2.24	325	60.0	0.36
0.69	2.44	451	70.6	1.00
0.69	6.29	477	64.7	1.00

Similar to what is commonly observed in other solar cells (e.g. Si, GaAs, etc.) at high injection, the increase in V_{oc} for all the cells in Table III was an exponential function of J_{sc}. This is shown in figure 16, where V_{oc} is plotted against J_{sc} for the cell with Eg=0.51 eV. Some researchers had speculated that the dislocation traps created by the lattice-mismatch between InGaAs and InP may be partially or fully passivated under high injection conditions, leading to higher than expected V_{oc} values. We did not observe any evidence of trap saturation, however. The experimental V_{oc} values measured at high injection, however, closely match the theoretical predictions made based on V_{oc} and J_{sc} values measured under low injection AM0 conditions, using standard solar cell equations.

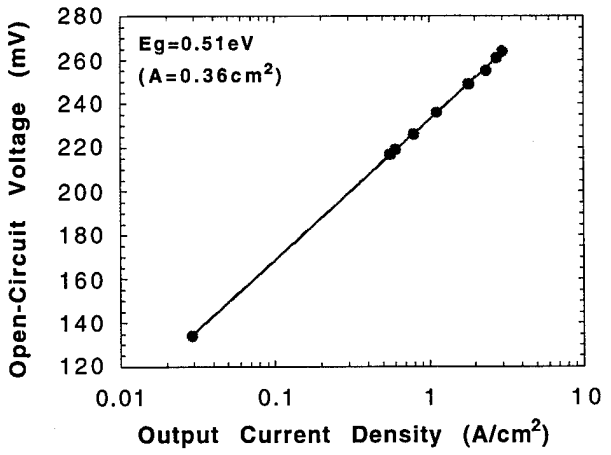

Figure 16.—Variation of V_{oc} with J_{sc} for the cell with Eg=0.51 eV (logarithmic curve fit shown).

The parameter most adversely affected by the parasitic series resistance is the fill factor. Initially, FF values increase with increasing light injection, due mainly to an increase in V_{oc}. Later, however the resistive power losses overtake this initial effect, and the FF values decrease at higher current levels. This is promarily due to the fact that the resistive power losses increase as a square function of the current, i.e. I^2R. A representative example of this behavior is shown in figure 17 for the cell with Eg=0.51 eV with a series resistance of about 20 mΩ. The I^2R losses in these cells can only become negligible if the total series resistance for each cell is kept below 5mΩ. For comparison, I-V curves are also shown for the cell with Eg=0.51 eV under AM0 and high injection conditions, in figures 18 and 19, respectively.

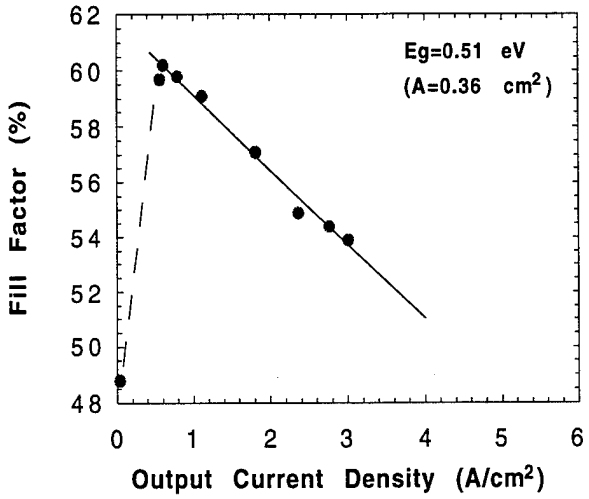

Figure 17.—Variation of FF with Jsc for the cell with Eg=0.51 eV (arbitrary curve fit shown).

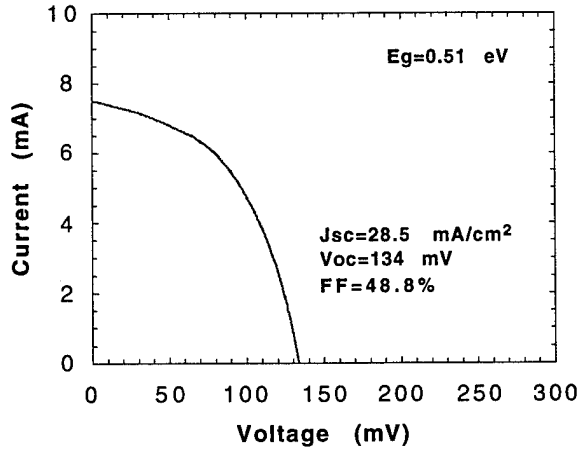

Figure 18.—AM0 I-V curve for the cell with Eg=0.51 eV.

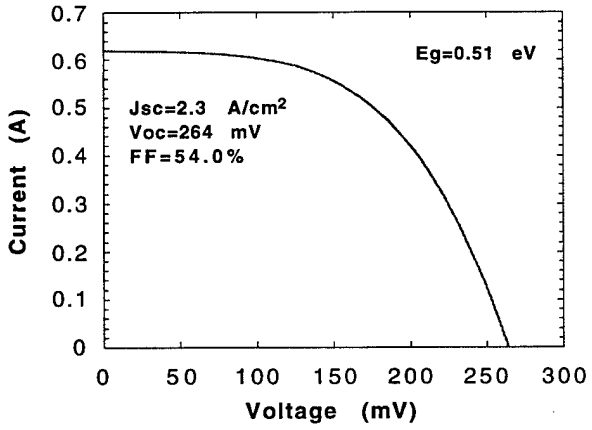

Figure 19.—High injection I-V curve for the cell with Eg=0.51 eV.

4.3.4. Hydrogen Passivation Data

The goal of the hydrogen passivation technique was to passivate the detrimental electrical characteristics of the crystalline defects created as a result of the growth of lattice-mismatched InGaAs layers on InP. To investigate the effects of the hydrogen passivation technique, half of an OMVPE growth run with Eg=0.57 eV was sent to Ohio State University for hydrogenation. Four PV cells were fabricated from hydrogenated samples. The other half was also processed into four cells but without hydrogenation. The performance of all eight cells were very similar under AM0 conditions. The AM0 results for the best cells from each half are given in Table IV.

Table IV.—AM0 I-V data (25 °C) for hydrogenated PV cells with Eg=0.51-0.69 eV.

H-Passivation	Cell Eg (eV)	J_{sc} (mA/ cm^2)	V_{oc} (mV)	FF (%)	Area (cm^2)
No	0.57	31.2	226	64.4	0.36
Yes	0.57	29.8	226	63.9	0.36

As shown in the table, effectively no improvements were observed in the performance of hydrogen passivated versus non-passivated cells. In order to assess the effects of hydrogenation further, spectral response and quantum efficiency measurements were also taken for the cells shown in Table IV. The results are given in figures 20 and 21, respectively. The data in these figures suggest that hydrogenation had essentially no effect on improving the cell response at any wavelength. As a result, no further hydrogen passivation work was carried out on other cells.

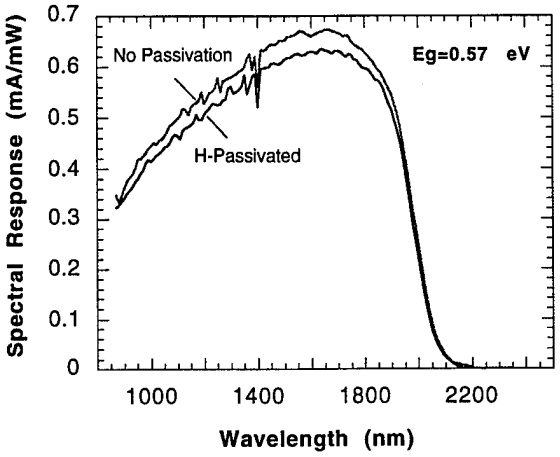

Figure 20.—Spectral response data for hydrogen-passivated and non-passivated cells.

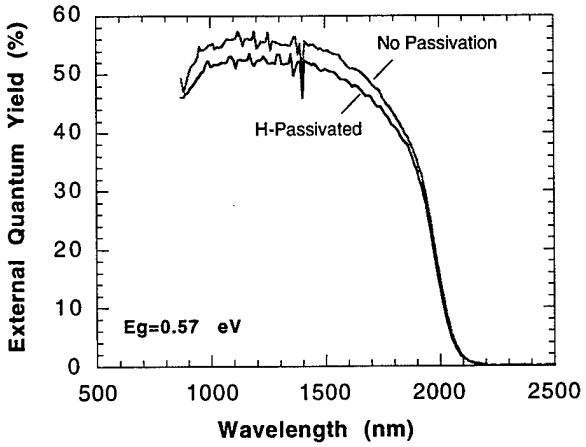

Figure 21.—Quantum efficiency data for hydrogen-passivated and non-passivated cells.

4.4. Thermal Storage

The thermal storage unit for STPV applications must absorb the heat from focused sunlight and radiate a near blackbody spectrum. For efficient TPV energy conversion, heat must be stored at very high temperatures (1500–1700 K). The temperature requirements push the state-of-the-art technology developed for solar dynamic power conversion. However, solar dynamic power conversion requires a working fluid to transfer the heat from the storage medium to the heat engine. In contrast, the coupling between the thermal storage unit and the TPV converter is radiative; hence, a working fluid is not required. This greatly simplifies the design, reduces the weight, and minimizes the effect of gravity on this technology. To prove the feasibility of thermal storage for STPV, we comprehensively researched existing thermal storage concepts, then adapted a high-temperature technique for use with STPV. An accurate description of the unit we propose to design and build in Phase II is a thermal storage/infrared radiator (TSIR).

One way to store heat is by using the latent heat of a phase-change material (PCM). Heat is stored as the PCM melts and is recovered as it resolidifies. A successful application of latent thermal storage is the solar dynamic heat receiver technology (SDHRT) designed to meet the electrical power requirements of the U. S. Space Station Freedom.[4] The receiver uses a LiF eutectic salt as the PCM. Metal canisters containing the PCM store excess thermal energy delivered to the system while the receiver is exposed to the sun. During the orbit night, stored energy is transferred through a working fluid to the heat engine. As a result, relatively stable power output is maintained throughout the entire orbit. The solar dynamic thermal storage unit is capable of storing heat at 1100 K. The receiver coupled with a heat engine is part of a prototype, 2 kW solar dynamic demonstrator developed at the NASA Lewis Research Center.

Unfortunately, the technology developed to store thermal energy for solar dynamic power conversion is difficult to push to 1500 K. Although fluoride eutectic salts can store significant quantities of thermal energy per unit mass, they have two distinct disadvantages. First, they have relatively low thermal conductivity. As a result, the size of each individual salt canister must be reduced and their numbers increased as the salt conductivity decreases. Second, these eutectic salts generally exhibit a large change in volume during solidification. As a result, voids are formed. Voids cause significant variations in the heat transfer rate and their formation is affected by gravity. It is critical to account for the effect when designing the thermal storage containment and projecting long-term reliability. The most limiting factor in pushing this technology to higher temperatures, however, is the lack of a reliable metal container to hold corrosive fluoride eutectic salts.

Fortunately, the Japanese have been developing a thermal storage technology capable of operating in the temperature range of 1100–1500 K.[5,6] Their technique employs a porous ceramic matrix entrained with fluoride salts. The salt/ceramic composite approach to thermal storage may be explained as microencapsulation of a PCM within the submicron pores of a ceramic matrix. The liquid salt is retained within the solid ceramic network by surface tension and capillary forces. Importantly, due to the high level of dispersion, void formation is suppressed. The lack of voids greatly simplifies the heat transfer and structural analyses, especially for space applications.

The porous ceramic matrix, usually silicon carbide (SiC), has a relatively high thermal conductivity, which greatly enhances heat transfer with the entrained salts. Heat storage occurs as latent heat of the PCM, and as sensible heat of the PCM and ceramic matrix. Therefore, the use of salt/ceramic composite represents not a pure latent heat, but a latent/sensible hybrid storage concept. Ultimately, this reduces the size and weight of the thermal storage unit relative to the technology developed for solar dynamic power generation.

Importantly for TPV technology, the use of a ceramic matrix allows containment of eutectic salts that solidify at higher temperatures. Porous SiC entrained with magnesium fluoride (MgF_2) is capable of operating at the temperature required for STPV: 1500 K.[7,8] The matrix/salt composite is fabricated by placing SiC with approximately 30% porosity in a moltem bath of salt in an inert atmosphere, such as nitrogen. A nonporous layer of SiC must then be attached to the surface to prevent evaporation of the salt during use. The surface layer may either be chemically vapor deposited, or machined from a solid piece and fitted like a sleave.

4.5. Stirling Solar Concentrator Dish Test Results

The solar concentrator located in the solar test facilities at McDonnell Douglas is comprised of 88 mirrors, each having an area of 1.0 m^2. It is capable of delivering a maximum of 80 kW of thermal energy to a target receiver with a concentration ratio of 15,000 suns. It can also achieve a concentration of 1000 suns uniformly over a 25 cm diameter spot. The concentrator is capable of generating estimated receiver temperatures of greater than 2500 °C on a small spot size.

The concentrated radiation density from the dish has a guassian distribution on the receiver. As a result, to achieve a more uniform temperature distribution, a SiC cavity was used for testing the dish (see figure 22). To be able to focus the concentrated light into the cavity openning, 72 of the 88 individual mirrors were covered up. Temperatures as high as 1350 °C (1623 K) were measured at the center of the receiver plate. Slight non-uniformity (~50 °C) was, however, observed across the receiver plate. The result of this solar dish testing demonstrates the feasibility of achieving the high temperatures (1500-1700 K) required for the development of a viable STPV system.

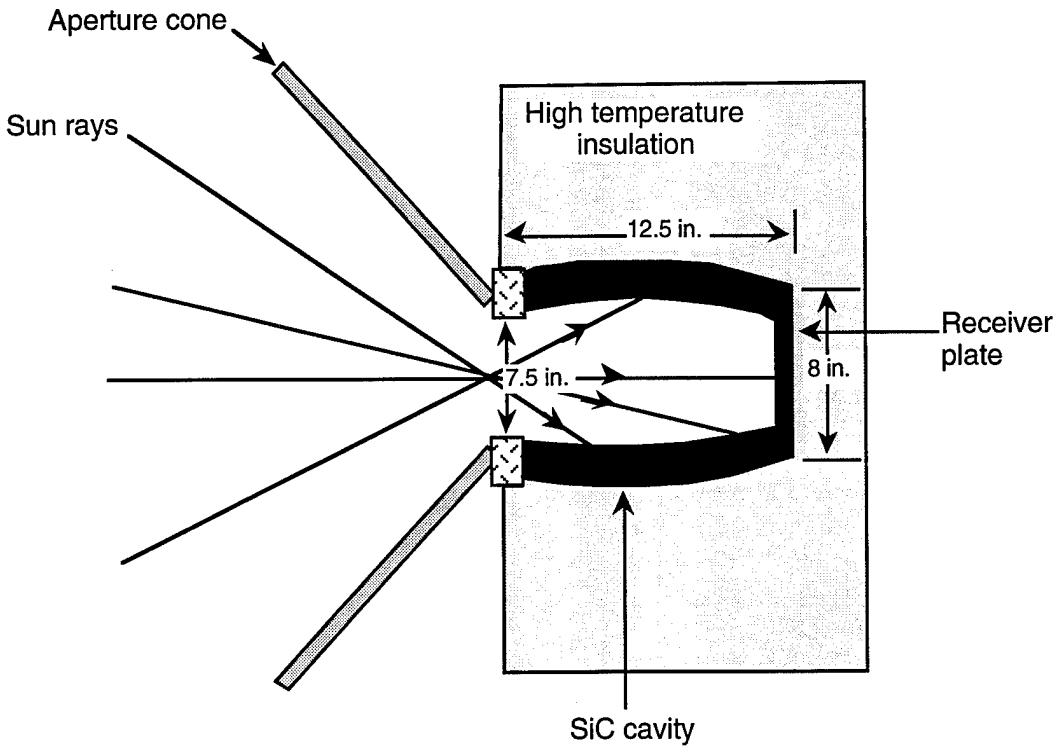

Figure 22.—The SiC cavity used for Stirling solar concentrator dish test.

4.6. Emitter, Bandpass/IR Reflector Filter, and PV Cell Converter Test Results

Four converter configurations were tested. Three selective emitters, Ho-YAG, Tm-(Lu,YAG), and Er-YAG were each coupled to a combination filter and PV cell matched to its peak radiative output. The Ho-YAG emitter was coupled with a combination bandpass/IR filter with λ_c=2.2 μm and a PV cell with Eg=0.51 eV. The Tm-(Lu, YAG) emitter was coupled with a combination filter with λ_c =2.0 μm and a PV cell with Eg=0.57 eV. And, the Er-YAG emitter was coupled to a combination filter with λ_c =1.7 μm and a PV cell with Eg=0.69 eV. The fourth configuration was a blackbody emitter coupled to a combination filter with λ_c =1.7 μm and a PV cell with Eg=0.69 eV. Also, since the PV cells with Eg=0.51 and 0.57 eV had no AR coatings, the output Jsc values used for converter calculations were multiplied by 1.35.

The center of the primary emission peaks for all three selective emitters closely coincide with the peak of the 1700 K blackbody spectrum. The PV cells with the lower bandgaps of 0.51 and 0.57 eV, exhibited inferior performance to the 0.69 eV cell. This is due to the increase in threading dislocation concentration with increased lattice mismatch. As a result, the converter with the Er-YAG emitter was not only more efficient, but it had a greater output power density than the converters with the Ho-YAG and the Tm-(Lu,YAG) emitters.

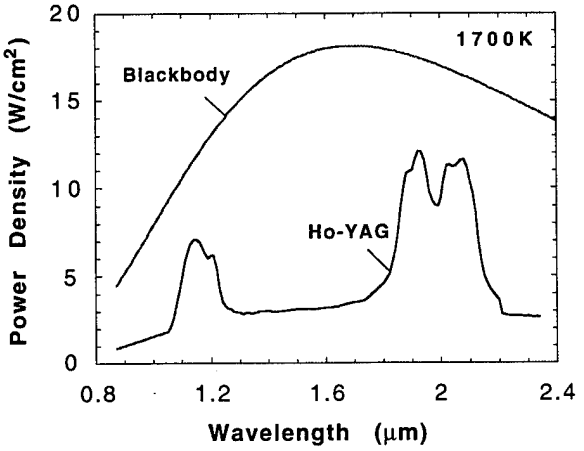

Figure 23.—Spectral irradiance data for the Ho-YAG selective emitter and a blackbody at 1700 K.

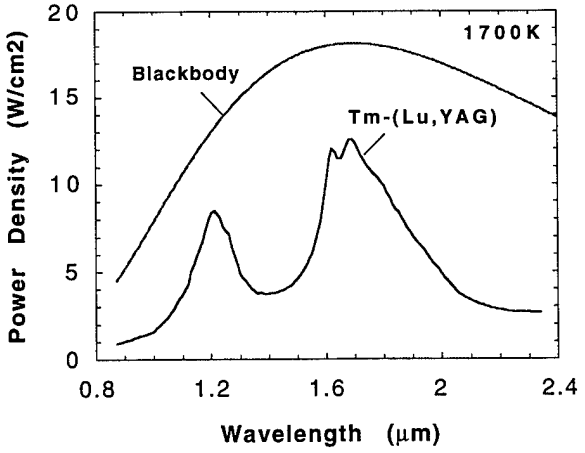

Figure 24.—Spectral irradiance data for the Tm-(Lu,YAG) selective emitter and a blackbody at 1700 K.

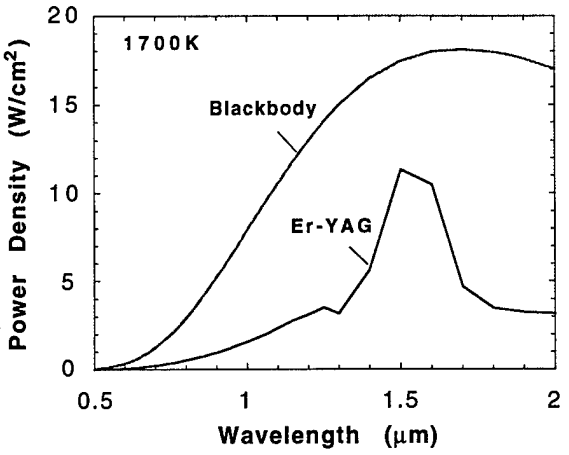

Figure 25.—Spectral irradiance data for the Er-YAG selective emitter and a blackbody at 1700 K.

Since the best selective emitter-based converter produced a relatively low output power density of 0.78 W/cm^2, a blackbody-based emitter converter was considered. The most efficient PV cell with Eg=0.69 eV, and the filter with λ_c=1.7 μm, were coupled to a blackbody emitter. The emittance of the blackbody emitter was assumed to be unity. This converter configuration resulted in the highest output power density. The test results for all four converters are presented below.

4.6.1 Ho-YAG Selective Emitter, Filter, and PV Cell with Eg=0.51 eV

The center of the emission peak for the Ho-YAG is well-tuned to the response of a PV cell with Eg=0.51 eV. This is illustrated in figure 25, where the filtered spectral irradiance of the emitter and the spectral response of the cell are shown. Following the testing methodology described in section 3.5, this converter produced an output power density of 0.29 W/cm^2 and a TPV conversion efficiency of 11.4%. The results are given in worksheet II.

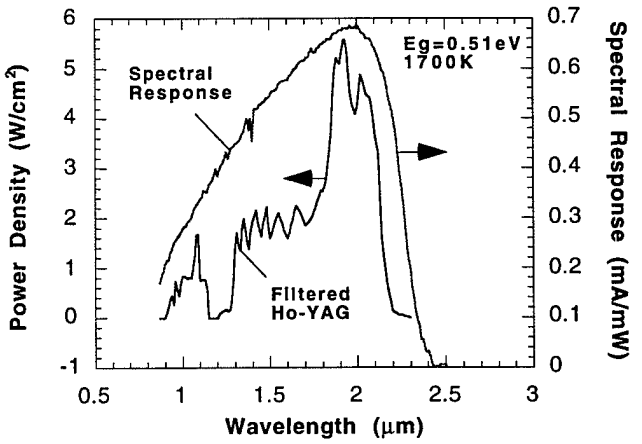

Figure 26.—Filtered spectral irradiance for the Ho-YAG selective emitter at 1700 K and the spectral response for the cell with Eg=0.51 eV.

Worksheet II.—Results for the converter with the PV cell with Eg=0.51 eV, bandpass/IR reflector filter with λc=2.2 μm, and the Ho-YAG selective emitter.

Description:						
Operating temperature		1700 K				
Selective Emitter		Ho-doped YAG			SE_Ho_A	
Filter		2.2 micron cut-off combination			F_2_2_A	
PV Cell		0.51 eV InGaAs			Cell_51_A	
Variable	**Value**	**Units**		**Variable**	**Value**	**Units**
Model Constants						
C_1	3.7390E+04	(W μm^4)/cm^2				
C_2	14388	μm K				
lambda_delta	0.01	μm				
System-level Inputs				**System-level Outputs**		
P_sys	100	W		nu_TPV_SE	11.40%	none
T_op	1700	K				
GFF	1	none				
Absorber Inputs				**Absorber Outputs**		
Absorber	SiC	none		e_absorb(λ)	see array data	W/(μm cm^2)
Spec		none		q_absorb	24.2122	W/cm^2
ε_absorb	1	none		P_absorb	8377.43	W
				A_absorb	346.00	cm^2
				e_emitter(λ)	see array data	W/(μm cm^2)
				q_emitter	7.0224	W/cm^2
				P_emitter	2429.76	W
				A_emitter	346.00	cm^2
Filter Inputs				**Filter Outputs**		
Filter		none		a_filter(λ)	see array data	none
Spec		none		e_intocell(λ)	see array data	W/(μm cm^2)
T_filter(λ)	see array data	none		q_intocell	2.534808	W/cm^2
R_filter(λ)	see array data	none		P_intocell	877.04355	W
PV Cell Inputs				**PV Cell Outputs**		
Cell		none		Jsc	1.52	A/cm^2
Spec		none		Jsc_arc	2.05	A/cm^2
Eg	0.51	eV		q_cell	0.29	W/cm^2
A_cell	1	cm^2		N_cell	346	none
SR_cell(λ)	see array data	A/(μm W)		A_array	346.00	cm^2
Voc	0.252	V				
FF	0.56	none				
GSF	0	none				
PF	1	none				

4.6.2 Tm-Lu,YAG Selective Emitter, Filter, and PV Cell with Eg=0.57 eV

PV cells with Eg=0.57 eV were fabricated to couple with the Tm-(Lu,YAG) selective emitter. The filtered spectral irradiance of this emitter and the spectral response of the cell are shown in figure 26. This converter demonstrated an output power density of 0.44 W/cm^2 and a TPV conversion efficiency of 16.2%. The results are shown in worksheet III.

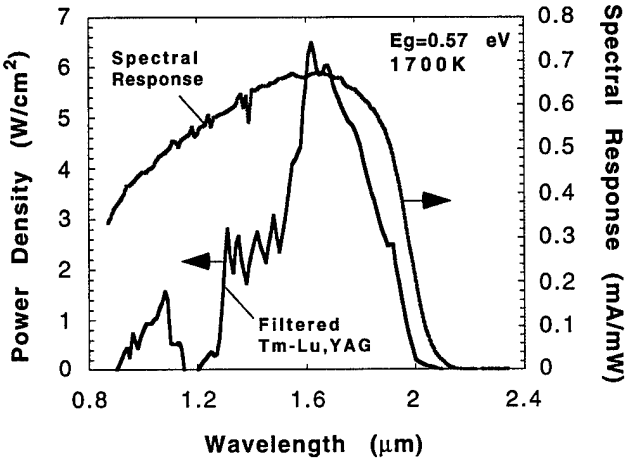

Figure 27.—Filtered spectral irradiance for the Tm-(Lu,YAG) selective emitter at 1700 K and the spectral response for the cell with Eg=0.57 eV.

Worksheet III.—Results for the converter with the PV cell with Eg=0.57 eV, bandpass/IR reflector filter with λc=2.0 μm, and the Tm-(Lu,YAG) selective emitter.

Description:						
Operating temperature		1700 K				
Selective Emitter		Tm-doped Lu,YAG			SE_Tm_A	
Filter		2.0 micron cut-off combination			F_2_0_A	
PV Cell		0.57 eV InGaAs			Cell_57_A	
Variable	**Value**	**Units**		**Variable**	**Value**	**Units**
Model Constants						
C_1	3.7390E+04	(W μm^4)/cm^2				
C_2	14388	μm K				
lambda_delta	0.01	μm				
System-level Inputs				**System-level Outputs**		
P_sys	100	W		nu_TPV_SE	16.20%	none
T_op	1700	K				
GFF	1	none				

Worksheet III.—Concluded.

Absorber Inputs			Absorber Outputs		
Absorber	SiC	none	e_absorb(λ)	see array data	W/(μm cm^2)
Spec		none	q_absorb	24.2122	W/cm^2
ε_absorb	1	none	P_absorb	5520.39	W
			A_absorb	228.00	cm^2
			e_emitter(λ)	see array data	W/(μm cm^2)
			q_emitter	8.0087	W/cm^2
			P_emitter	1825.99	W
			A_emitter	228.00	cm^2
Filter Inputs			**Filter Outputs**		
Filter		none	a_filter(λ)	see array data	none
Spec		none	e_intocell(λ)	see array data	W/(μm cm^2)
T_filter(λ)	see array data	none	q_intocell	2.7073887	W/cm^2
R_filter(λ)	see array data	none	P_intocell	617.28462	W
PV Cell Inputs			**PV Cell Outputs**		
Cell		none	Jsc	1.67	A/cm^2
Spec		none	Jsc_arc	2.25	A/cm^2
Eg	0.57	eV	q_cell	0.44	W/cm^2
A_cell	1	cm^2	N_cell	228	none
SR_cell(λ)	see array data	A/(μm W)	A_array	228.00	cm^2
Voc	0.325	V			
FF	0.6	none			
GSF	0	none			
PF	1	none			

4.6.3 Er-YAG Selective Emitter, Filter, and PV Cell with Eg=0.69 eV

The filtered spectral irradiance of Er-YAG and the spectral response of the best cell with Eg=0.69 eV are shown in figure 27. As with the previous converters, the cell response is well-matched to the emission peak of the selective emitter. Because of the superior spectral response of the cell, this converter demonstrated the best performance of those based on selective emitters: an output power density of 0.78 W/cm^2 and a TPV conversion efficiency of 29.0%. The results are given in worksheet IV.

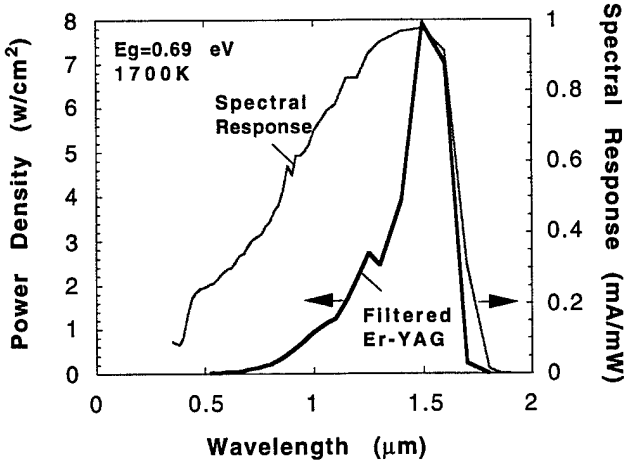

Figure 28.—Filtered spectral irradiance for the Er-YAG selective emitter at 1700 K and the spectral response for the cell with Eg=0.69 eV.

Worksheet IV.—Results for the converter with the PV cell with Eg=0.69 eV, bandpass/IR reflector filter with λc=1.7 μm, and the Er-YAG selective emitter.

Description:							
	Operating temperature		1700 K				
	Selective Emitter		Er-doped YAG		SE_Er_A		
	Filter		1.7 micron cut-off combination		F_1_7_A		
	PV Cell		0.69 eV InGaAs		Cell_69_B		
	Variable	**Value**	**Units**	**Variable**	**Value**	**Units**	
Model Constants							
	C_1	3.7390E+04	(W μm^4)/cm^2				
	C_2	14388	μm K				
	lambda_delta	0.01	μm				
System-level Inputs				**System-level Outputs**			
	P_sys	100	W	nu_TPV_SE	29.00%	none	
	T_op	1700	K				
	GFF	1	none				

Worksheet IV.—Concluded.

Absorber Inputs			**Absorber Outputs**			
Absorber	SiC	none	e_absorb(λ)	see array data	W/(μm cm^2)	
Spec		none	q_absorb	24.2122	W/cm^2	
ε_absorb	1	none	P_absorb	3123.38	W	
			A_absorb	129.00	cm^2	
			e_emitter(λ)	see array data	W/(μm cm^2)	
			q_emitter	6.6471	W/cm^2	
			P_emitter	857.47	W	
			A_emitter	129.00	cm^2	
Filter Inputs			**Filter Outputs**			
Filter		none	a_filter(λ)	see array data	none	
Spec		none	e_intocell(λ)	see array data	W/(μm cm^2)	
T_filter(λ)	see array data	none	q_intocell	2.4282264	W/cm^2	
R_filter(λ)	see array data	none	P_intocell	313.2412	W	
PV Cell Inputs			**PV Cell Outputs**			
Cell		none	Jsc	2.44	A/cm^2	
Spec		none	Jsc_arc	2.44	A/cm^2	Cell already AR coated!
Eg	0.69	eV	q_cell	0.78	W/cm^2	
A_cell	1	cm^2	N_cell	129	none	
SR_cell(λ)	see array data	A/(μm W)	A_array	129.00	cm^2	
Voc	0.451	V				
FF	0.706	none				
GSF	0	none				
PF	1	none				

4.6.4 Blackbody Broadband Emitter, Filter, and PV Cell with Eg=0.69 eV

The final converter configuration consisted of a blackbody emitter, a bandpass/IR reflector filter (λ_c=1.7 μm), and a PV cell with Eg=0.69 eV. The filtered spectral irradiance of a blackbody emitter and the spectral response of the best cell with Eg=0.69 eV are shown in figure 28. This converter produced an output power density of 1.94 W/cm^2 and an efficiency of 26.9%. The results are shown in worksheet V.

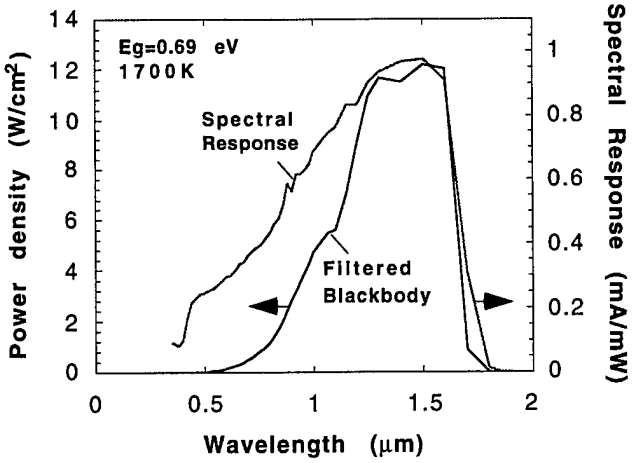

Figure 29.—Filtered spectral irradiance for a blackbody emitter at 1700 K and the spectral response for the cell with Eg=0.69 eV.

Worksheet V.—Results for the converter with the PV cell with Eg=0.69 eV, bandpass/IR reflector filter with λ_c=1.7 μm, and a blackbody emitter.

Description:							
Operating temperature		1700 K					
Selective Emitter		None			None		
Filter		1.7 micron cut-off combination			F_1_7_A		
PV Cell		0.69 eV InGaAs			Cell_69_B		
Variable	**Value**	**Units**		**Variable**	**Value**	**Units**	
Model Constants							
C_1	3.7390E+04	(W μm^4)/cm^2					
C_2	14388	μm K					
lambda_delta	0.01	μm					
System-level Inputs				**System-level Outputs**			
P_sys	100	W		nu_TPV_SE	26.90%	none	
T_op	1700	K					
GFF	1	none					

Worksheet V.—Concluded.

Absorber Inputs				Absorber Outputs			
Absorber	SiC		none	e_absorb(λ)	see array data	W/(μm cm^2)	
Spec			none	q_absorb	24.2122	W/cm^2	
ε_absorb		1	none	P_absorb	1259.04	W	
				A_absorb	52.00	cm^2	
				e_emitter(λ)	see array data	W/(μm cm^2)	
				q_emitter	24.2122	W/cm^2	
				P_emitter	1259.04	W	
				A_emitter	52.00	cm^2	
Filter Inputs				**Filter Outputs**			
Filter			none	a_filter(λ)	see array data	none	
Spec			none	e_intocell(λ)	see array data	W/(μm cm^2)	
T_filter(λ)	see array data		none	q_intocell	7.22	W/cm^2	
R_filter(λ)	see array data		none	P_intocell	375.44	W	
PV Cell Inputs				**PV Cell Outputs**			
Cell			none	Jsc	6.29	A/cm^2	
Spec			none	Jsc_arc	6.29	A/cm^2	Cell already AR coated!
Eg		0.69	eV	q_cell	1.94	W/cm^2	
A_cell		1	cm^2	N_cell	52	none	
SR_cell(λ)	see array data		A/(μm W)	A_array	52.00	cm^2	
Voc		0.477	V				
FF		0.647	none				
GSF		0	none				
PF		1	none				

Because of the high current output density (6.29 A/cm^2) of this converter, the PV cell (Eg=0.69 eV) exhibited a rather low FF, i.e. 64.7%. As explained in section 4.3.3, resistive power losses become significant at high output currents. The theoretically calculated Rs for this cell was 14 mΩ.[9] Lower values of Rs can increase the FF, and therefore the output power density and efficiency, rather dramatically. This effect is shown in Table V, where the theoretically calculated FF, output power density, and efficiency values are given as the series resistance of the cell with Eg=0.69 eV is varied.

Table V.—The effect of Rs on the performance of the converter with the blackbody emitter for the cell with Eg=0.69 eV.

Rs (mΩ)	FF (%)	Pout (W/cm^2)	Efficiency (%)
0	79.6	2.39	33.1
5	74.4	2.23	30.9
10	69.1	2.07	28.7
14	64.7	1.94	26.9
20	58.6	1.76	24.4

As shown in the table, small variations in Rs can effect large changes in converter output power density and efficiency. Minor modifications in the doping density and thickness of the OMVPE grown layers in the InGaAs/InP PV cell structure can indeed result in the achievement of Rs values at or below 5 mΩ. Practical converter output power densities and TPV conversion efficiencies greater than 2.23 W/cm^2 and 30.9%, respectively, are therefore possible with this converter configuration. In addition, it is expected that optimized and more efficient PV cells with Eg=0.69 eV can be fabricated during the Phase II period, further improving the performance of this converter design.

The performance of all four converters discussed above is summarized in Table VI.

Table VI.—TPV Converter output power density and efficiency data for a source temperature of 1700 K.

Emitter	Filter λc (μm)	PV Cell Eg (eV)	Pout (W/cm^2)	Efficiency (%)
Ho-YAG	2.2	0.51	0.29	11.4
Tm-Lu,YAG	2.0	0.57	0.44	16.2
Er-YAG	1.7	0.69	0.78	29.0
Blackbody	1.7	0.69	1.94	26.9

5. Conclusions

The results of our Phase I effort have successfully demonstrated that very efficient converters with high output power densities can be realized for STPV applications. The following specific conclusions are also drawn from our work:

1. Higher bandgap InGaAs/InP PV cells performed far better than the lower bandgap cells. As a result, the converter with the Er-YAG selective emitters showed a superior performance than the converters with the Ho-YAG and the Tm-(Lu,YAG) selective emitters.

2. Even though the converter with the Er-YAG selective emitter was highly efficient, its output power density was insufficient to enable the fabrication of a practical, cost-effective STPV system.

3. The converter with the filtered blackbody emitter was both very efficient and had a high output power density (~2 W/cm^2).

4. By improving the PV cell and filter performance blackbody-based STPV converters can be developed with TPV conversion efficiencies exceeding 30% and output power densities over 2 W/cm^2.

Finally, the results of our Phase I project show the feasibility of the development of an STPV system with a practical total system efficiency of greater than 20% and an output power density of about 2 W/cm^2.

6. Future Research and Development

Based on the work performed in Phase I, two prototype STPV systems will be designed and evaluated in Phase II. One prototype will use the conventional PV cell technology, while the other will use the advanced monolithic integrated module (MIM) cell technology. Both systems will be superior to planar solar arrays or linear concentrator solar arrays for space-based power generation. Specifically, they will be designed for a lifespan of 5 to 7 years, an output power level of 50 W electric (EOL), and a specific power of better than 100 W/kg. Linear concentrator solar arrays are presently being studied by BMDO. They are projected to have a BOL efficiency of about 20% without energy storage. The STPV systems, which will be built in Phase II, will have comparable efficiency but with energy storage. Additionally, the thermal storage/IR receiver (TSIR) unit associated with STPV will be less costly and lighter than batteries, which improves the specific power, reliability, and lifespan.

Specific objectives for Phase II research and development are given below:

1. demonstrate an STPV prototype generating 50 We—alpha prototype

   An STPV prototype will be designed and fabricated. It will be comprised of a SiC thermal absorber/emitter cavity, filters, and conventional InGaAs/InP PV cell strings. This unit will not have energy storage capability. It will be tested in the Stirling solar concentrator dish.

2. develop the MIM fabrication technology

   The processing and fabrication procedures for MIM will be developed. MIM strings will be fabricated and tested.

3. design, build and test the TSIR unit

The thermal storage unit will be designed with the aid of numerical analysis techniques. The construction techniques for its fabrication will be studied and optimized. A unit will be manufactured and bench tested.

4. demonstrate an STPV unit with MIM technology and thermal storage—beta prototype

The technologies developed in the objectives 2 and 3 above will be used to design and construct the second prototype. The use of MIM instead of conventional modules should eliminate the need to include filters in this prototype. This advanced unit with thermal storage capability will tested in the Stirling solar concentrator dish.

The time line for Phase II research is outlined in the Ghant chart below:

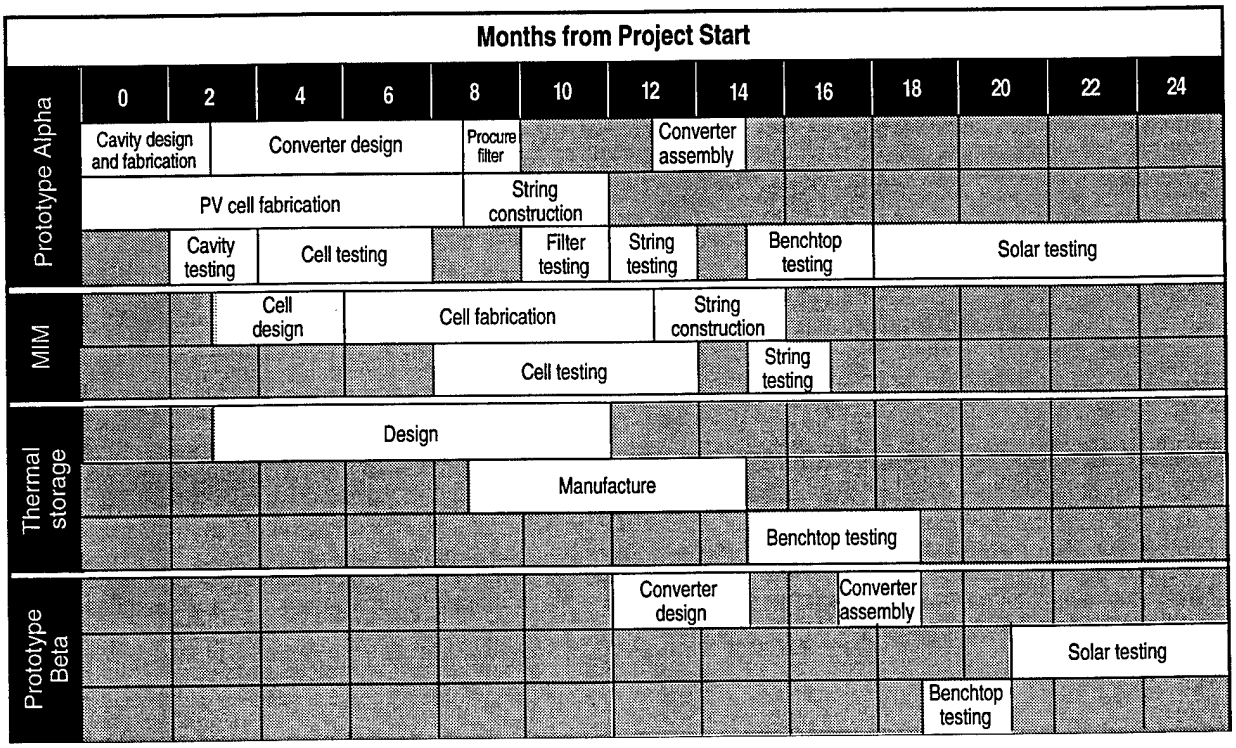

7. References

[1] K.W. Stone, S.M. Kusek, R.E. Drubka, and T.D. Fay, "Analysis of Thermophotovoltaic Test Data From Experiments Performed at McDonnell Douglas", The First NREL Conference on Thermophotovoltaic Generation of Electricity, Copper Mountain, CO July 24–27, 1994.

[2] N.S. Fatemi and V.G. Weizer, "On the Electrical and Metallurgical Behavior of AuZn Contacts to p-type InP." J. Appl. Phys. Lett. **77**, 5241, 1995.

[3] V.G. Weizer and N.S. Fatemi, "A Simple, Extremely Low Resistance Contact System to n-InP that does not Exhibit Metal-Semiconductor Intermixing During Sintering." Appl. Phys. Lett. **62**, 2731, 1993.

[4] Leigh M. Sedgwick, "Solar Dynamic Heat Receiver Technology Final Report", prepared for NASA Lewis Research Center by the Boeing Company Seattle, WA, January 1991.

[5] Y. Takahashi et. al., "High Temperature Fluoride Composites for Latent Thermal Storage in Advanced Space Solar Dynamic System", Proceedings of the 24th Intersociety Energy Conversion Engineering Conference IECEC-89, IEEE, New York, N.Y., USA, 1989.

[6] Y. Takahashi et. al., "Thermoanalytical Investigation of Fluoride Composites for Latent Thermal Storage", presented at the Second Japan-China Joint Symposium on Calorimetry and Thermal Analysis, 30 May—1 June 1990, Osaka, Japan, Elsevier Science Publishers B.V., Amsterdam, 1991.

[7] Ajay K. Misra and John D. Whittenberger, "Estimated Heats of Fusion of Fluoride Salt Mixtures Suitable for Thermal Energy Storage Applications", NASA Technical Memorandum 87320, May 1986.

[8] K. Tanaka, "Preliminary Examination of Latent Heat-Thermal Energy Source Materials III. Screening of Eutectic Mixtures over a Range from 200 to 1500 °C", Bul. Electrotech. Lab., Vol. 51, No. 7, pp. 19–33, 1987.

[9] Martin A. Green, "Solar Cells Operating Principles, Technology, and System Applications", Prentice-Hall, pp. 96–97.

REPORT DOCUMENTATION PAGE

Form Approved
OMB No. 0704-0188

1. AGENCY USE ONLY (*Leave blank*)	2. REPORT DATE	3. REPORT TYPE AND DATES COVERED
	February 9, 1996	Final Contractor Report

4. TITLE AND SUBTITLE

A Solar Thermophotovoltaic Electrical Gnerator for Remote Power Applications

5. FUNDING NUMBERS

NAS3–27779

6. AUTHOR(S)

Navid S. Fatemi

7. PERFORMING ORGANIZATION NAME(S) AND ADDRESS(ES)

Essential Research, Inc.
2460 Fairmount Blvd., Suite A
Cleveland, Ohio 44106

8. PERFORMING ORGANIZATION REPORT NUMBER

9. SPONSORING/MONITORING AGENCY NAME(S) AND ADDRESS(ES)

National Aeronautics and Space Administration
Lewis Research Center
Cleveland, Ohio 44135–3191

10. SPONSORING/MONITORING AGENCY REPORT NUMBER

11. SUPPLEMENTARY NOTES

12a. DISTRIBUTION/AVAILABILITY STATEMENT

Unclassified - Unlimited

12b. DISTRIBUTION CODE

13. ABSTRACT *(Maximum 200 words)*

This final report presents the results of an SBIR Phase I project. Several TPV converters were fabricated and tested. The converters consisted of rare-earth-doped yttrium aluminum garnet (YAG) and Lutetium yttrium aluminum garnet (Lu,YAG) selective emitters and a blackbody emitter, bandpass/infrared (IR) reflector filters, and InGaAs photovoltaic (PV) cells. The operating temperature of the heat source was 1700 K. The filtered blackbody-based converter was found to be the most suitable candidate for Solar TPV applications as compared to selective emitter-based converters. High output power density (~2 W/cm^2) and efficiency (26.9%) were observed for this converter. The results of our Phase I project show the feasibility of the development of an STPV system with a practical total system efficiency of greater than 20% and an output power density of about 2 W/cm^2.

14. SUBJECT TERMS

Solar thermophotovoltaics; Electrical power generation; Remote power

15. NUMBER OF PAGES

35

16. PRICE CODE

17. SECURITY CLASSIFICATION OF REPORT	18. SECURITY CLASSIFICATION OF THIS PAGE	19. SECURITY CLASSIFICATION OF ABSTRACT	20. LIMITATION OF ABSTRACT
Unclassified	Unclassified	Unclassified	